

Article

The Use of the Surface Roughness Value to Quantify the Extent of Supercritical CO₂ Involved Geochemical Reaction at a CO₂ Sequestration Site

Jinyoung Park ¹, Kyoungbae Baek ², Minhee Lee ^{2,*}, Chul-Woo Chung ³ and Sookyun Wang ⁴

¹ Petroleum and Marine Research Division, Korea Institute of Geoscience and Mineral Resources, Daejeon 34132, Korea; pjy9614@kigam.re.kr

² Department of Earth Environmental Sciences, Pukyong National University, 45 Yongso-ro, Nam-gu, Busan 48513, Korea; darkbkb@kcl.re.kr

³ Department of Architectural Engineering, Pukyong National University, 45 Yongso-ro, Nam-gu, Busan 48513, Korea; cwchung@pknu.ac.kr

⁴ Department of Energy Resources Engineering, Pukyong National University, 45 Yongso-ro, Nam-gu, Busan 48513, Korea; sookyun@pknu.ac.kr

* Correspondence: heelee@pknu.ac.kr; Tel.: +82-51-629-6630

Academic Editor: Jose Augusto Paixao Coelho

Received: 21 April 2017; Accepted: 22 May 2017; Published: 2 June 2017

Abstract: Changes in the physical properties of the supercritical CO₂ (scCO₂) reservoir rock is one of the most important factors in controlling the storage safety at a scCO₂ sequestration site. According to recent studies, it is probable that geochemical reactions influence changes in the rock properties after a CO₂ injection in the subsurface, but quantitative data that reveal the interrelationship of the factors involved and the parameters needed to evaluate the extent of scCO₂-rock-groundwater reactions have not yet been presented. In this study, the potential for employing the surface roughness value (SR_{RMS}) to quantify the extent of the scCO₂ involved reaction was evaluated by lab-scale experiments. For a total of 150 days of a simulation of the scCO₂-sandstone-groundwater reaction at 100 bar and 50 °C, the trends in changes in the physical rock properties, pH change, and cation concentration change followed similar logarithmic patterns that were significantly correlated with the logarithmic increase in the SR_{RMS} value. These findings suggest that changes in surface roughness can quantify the extent of the geochemical weathering process and can be used to evaluate leakage safety due to the progressive changes in rock properties at scCO₂ storage sites.

Keywords: CO₂ sequestration; CO₂ reservoir rock; leakage safety; scCO₂-water-rock reaction; surface roughness value; supercritical CO₂

1. Introduction

Various CO₂ capture and sequestration technologies have been developed to reduce CO₂ emissions and the International Energy Agency (IEA) has announced that CO₂ capture and sequestration (CCS) technology will cover 19% of the total CO₂ reductions by 2050 [1–6]. Among them, geological sequestration will be deeply considered to reduce CO₂ emissions at low cost [7–11]. Several CO₂ sequestration projects in the world have been successfully conducted [12–15], but some CO₂ injection sites were found to be impractical, even though their site characterization, such as geophysical exploration, geo-structural investigation, and drilling core analysis, was thoroughly conducted [16,17]. For successful CO₂ sequestration in heterogeneous subsurface formations, the practicability of the CO₂ sequestration process based on storage capacity and leakage prevention should be guaranteed before the field scale CO₂ injection. The previous research over the last two decades revealed that the injection of supercritical CO₂ (scCO₂) into a reservoir rock initiates a geochemical reaction in

the scCO₂-rock-groundwater system, but it does not threaten the storage safety of CO₂ reservoir formations because of its long reaction time [18–20]. However, in the past five years, several studies have cast doubts on whether the rate of the scCO₂-rock-groundwater reaction is too slow to affect the change of CO₂ storage capacity and leakage safety after scCO₂ injection [21–26].

If there exists the possibility of a fast reaction, and thus the geochemical reaction is one of the more important parameters controlling CO₂ storage and leakage safety, then a quantitative understanding of the scCO₂-rock-groundwater reaction occurring in the CO₂ storage site is essential for successful CO₂ sequestration in the subsurface [27–29]. Over the last decade, meaningful information about what kinds of geochemical reactions dominate in CO₂ sequestration sites have been qualitatively acquired through laboratory scale experiments, but most of these have been limited to qualitative investigations such as compositional and/or mineralogical analyses [30–36]. These results verified only the occurrence of a geochemical reaction at the CO₂ sequestration system, and they were limited in providing the extent of the reaction or discovering its influence on sequestration capacity, such as leakage or storage capacity, because it is difficult to reenact the geochemical reaction occurring at a CO₂ storage site and also to determine the interrelationship between the geochemical reaction and the other property changes of the reservoir rock [37–39]. It is now more important than ever to search for the available CO₂ reservoir sites in the subsurface locations and to prevent the accidental leakage of CO₂ originating from a geochemical reaction. However, the development of a new quantitative parameter for evaluating the scCO₂ involved geochemical reaction in sequestration conditions has almost never been attempted in previous studies [40,41].

The present study focuses on the quantitative investigation of the scCO₂ involved reaction occurring at CO₂ storage sites and provides the potential use of changes in surface roughness of the CO₂ reservoir rock to quantify the extent of the scCO₂-reservoir rock-groundwater reaction. The interrelationship among property changes originating from the geochemical reaction is also bound to be revealed by the laboratory scale experiments. This is a novel approach to developing a quantitative technique that uses the surface roughness to investigate the scCO₂-rock-groundwater reaction and also to evaluate the long-term rock property changes originating from the geochemical reaction in scCO₂ storage conditions. The results of this study will provide ideas for the development of a method for safety estimation based on the extent of the geochemical reaction in a CO₂ sequestration site and of a future plan for strengthening the successful confrontation technology for CO₂ leakage.

2. Materials and Methods

2.1. Sandstone Cores and Groundwater Samples

Currently, South Korea is ranked seventh in the world in terms of CO₂ emissions, having produced a total of 739 megatons in 2011 alone [42], and the Korean government currently plans to inject more than 100 megatons of CO₂ into the subsurface by 2020 [43]. From a previous study, the Sindong lithostratigraphic group of the Gyeongsang basin was considered as an available CO₂ storage site on the Korean peninsula (CO₂ storage capacity of 1011 megatons) [44]. In 2014, the Gyeongsang basin was announced as one of the candidate sites for a scCO₂ storage test in Korea, and continuous drill cores (4.2 cm of average diameter) were collected at two drilling sites (average 1200 m in depth). From the property analysis of these cores, three coarse sandstone formations (850, 1000, and 1050 m in depth) with medium porosity (porosity of 7.0%–9.8%) and moderate thickness (total of 100 m) were found, and their sandstone cores (S1, S2, and S3) were used for this study. A total of nine consolidated cylindrical sandstone cores (each 4.2 cm in diameter and 6–7 cm in length) without cracks or fractures were used to measure the physical and geochemical property changes of the cores during the scCO₂-water-core reaction. For each sandstone core, several thin slabs (1 × 1 × 0.2 cm each) were additionally prepared to observe the surface roughness change and the cation concentration change for the whole reaction time. The geological map around the drilling site, the sandstone core, and the slab used for the experiment are shown in Figure 1. The mineral composition of each core was identified

by modal analysis and more than 500 locations on each thin section surface were observed using the point counter attached in a polarizing microscope.

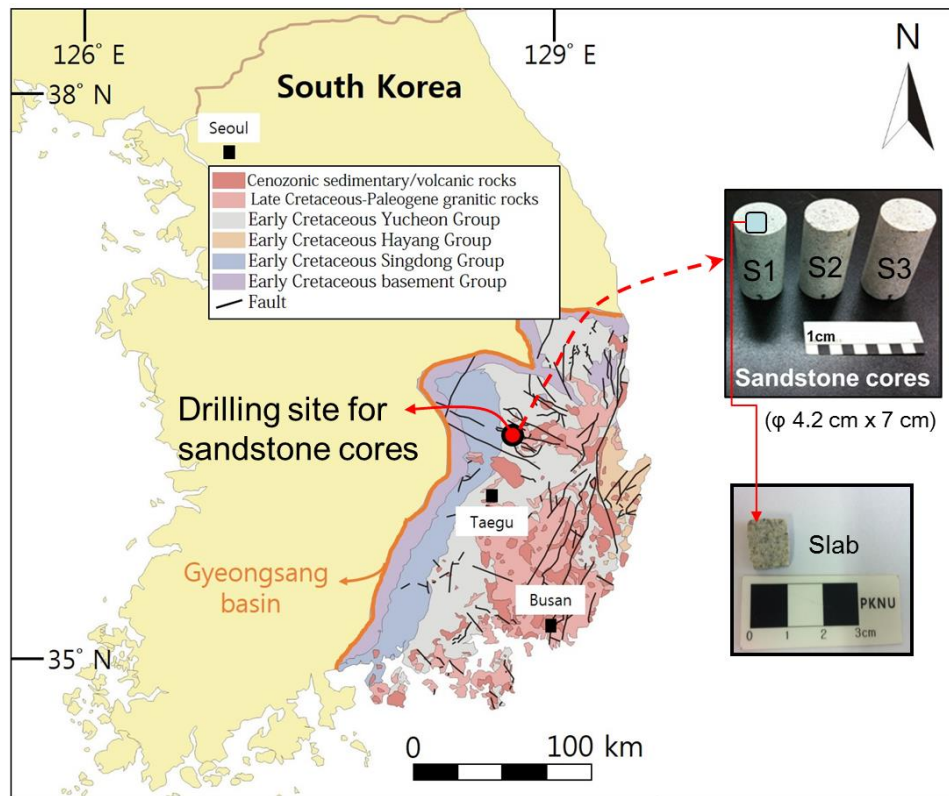


Figure 1. Geological map around the drilling site (●) and photographs of sandstone cores and a slab for the experiment (modified from [22]).

The results of the modal analysis for the three cores (S1, S2, and S3) reveal that the sandstone surface is mostly composed of quartz, perthite, plagioclase, calcite, muscovite, biotite, and chlorite, and their average proportions were 47.4%, 18.5%, 10.5%, 5.4%, 1.7%, 1.5%, and 1.4%, respectively (Table 1). The surface roughness changes for these seven minerals were specifically targeted during the experiment.

Table 1. Petrographic detrital modal analysis for sandstones.

Thin Section No.	Mineral Portion (%)							
	Quartz	Plagioclase	K-Feldspar	Muscovite	Biotite	Calcite	Chlorite	Others
S1-1	50.7	7.8	25.5	0.3	2.3	3.1	3.1	7.2
S1-2	43.4	9.2	27.6	0.3	1.5	5.3	5.1	7.6
S1-3	50.5	11.3	23.5	1.1	0.2	4.3	3.2	5.9
S1-4	46.1	8.1	23.2	1.4	2.1	6.2	4.7	8.2
Average ± standard deviation	47.7 ± 3.6	9.1 ± 1.6	25.0 ± 2.0	0.8 ± 0.6	1.5 ± 0.9	4.7 ± 1.3	4.0 ± 1.0	7.2 ± 1.0
S2-1	38.7	13.4	17.9	0.7	2.2	9.5	0.1	17.5
S2-2	35.6	15.5	13.4	1.5	2.7	12.4	0.0	18.9
S2-3	40.5	11.7	16.9	0.1	1.4	6.4	0.0	23.0
S2-4	41.9	16.8	19.8	1.4	1.9	4.1	0.1	14.0
Average ± standard deviation	39.2 ± 2.7	14.4 ± 2.3	17.0 ± 2.7	0.9 ± 0.7	2.1 ± 0.5	8.1 ± 3.6	0.1 ± 0.1	18.4 ± 3.7
S3-1	61.6	7.6	13.2	3.3	0.4	0.3	0.1	13.5
S3-2	57.5	5.1	7.7	5.9	0.6	3.5	0.3	19.4
S3-3	55.1	8.7	14.3	2.7	0.4	3.8	0.2	14.8
Average ± standard deviation	58.1 ± 3.3	7.1 ± 1.8	11.7 ± 3.5	4.0 ± 1.7	0.5 ± 0.1	2.5 ± 1.9	0.2 ± 0.1	15.9 ± 3.1

Groundwater was sampled from a monitoring well near the drilling site (>400 m in depth) and analytical results for the groundwater quality are shown in Table 2. The concentrations of Na^+ and Cl^- were higher than those of fresh water, suggesting the groundwater was mixed with sea water below the drilling site.

Table 2. Temperature, pH, and chemical composition of groundwater used in the experiment.

Temp. (°C)	pH	Average Concentration (mg/L)										
		Na^+	Ca^{2+}	K^+	Mg^{2+}	Si^{4+}	Al^{3+}	Fe^{2+}	Cl^-	SO_4^{2-}	NO_3^-	HCO_3^-
40.6	8.6	633.2	547.1	23.3	20.9	12.4	4.3	0.0	2109.1	259.3	212.0	51.7

2.2. Measurement of the Surface Roughness Value for Sandstone Slabs

The identification of the scCO_2 -rock-pore water geochemical reaction at scCO_2 sequestration conditions has been studied by various analytical processes. These approaches include qualitative processes mostly depending on visual inspection or compositional analysis using SEM/EDS (Scanning Electron Microscope/Energy Dispersive X-ray Spectrometer; VEGA II LSU, Tescan, Brno, Czech Republic), XRD (X-ray Diffractometer; X'Pert-MPD, Philips, Eindhoven, The Netherlands), and XRF (X-ray Fluorescence Spectrometer; XRF-1800, Shimadzu, Kyoto, Japan) [45,46]. However, quantitative information acquired from this study was very limited, such as in mineral composition transfer and structural change [47,48]. To supplement these limitations, the surface roughness change of the rock surface during the scCO_2 -sandstone-groundwater reaction was investigated, and the feasibility of its use as a parameter to evaluate the geochemical weathering process was verified by comparing the physical property change of the sandstone with the cation concentration change in groundwater during the geochemical reaction.

To observe the surface roughness change of the slab surface over the reaction time, one surface of each slab prepared from the sandstone core was polished with diamond-coated paper and the other slab surface was attached to a glass slide plate with epoxy resin. After being washed with methanol, each thin slab was placed at the bottom of a Teflon beaker, which was fixed inside a high pressurized stainless steel cell (with a capacity of 150 mL), and 100 mL of groundwater was poured into the Teflon beaker. The inside of the cell was pressurized up to 100 bar using a high-pressure syringe pump (Isco-D260, TELEDYNE ISCO, Lincoln, NE, USA) and the empty space in the cell was filled with scCO_2 by a gas flow regulator attached to a high-pressure syringe pump. Each cell was placed in an oven to maintain a constant temperature of 50 °C, which led to a scCO_2 -rock-groundwater reaction in the cell at scCO_2 sequestration conditions. The scCO_2 -sandstone slab-groundwater reaction in the cell was executed at 100 bar and 50 °C for 150 days and the apparatus of the slab experiment is shown in Figure 2.

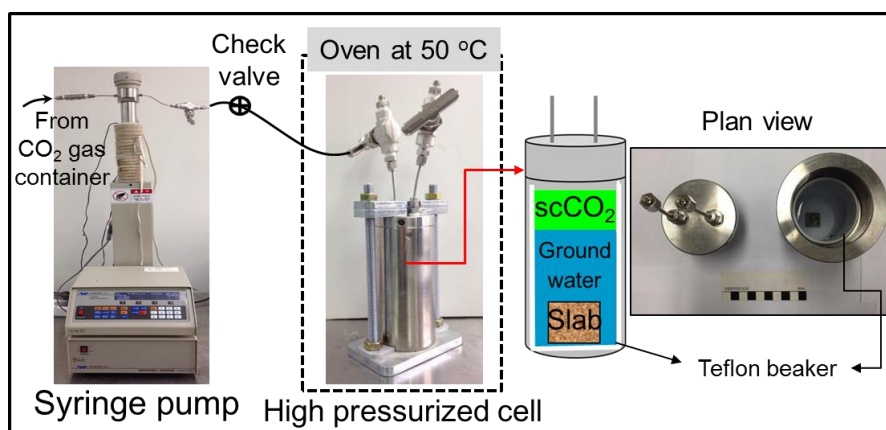


Figure 2. Apparatus used for the slab experiment to simulate the scCO_2 -sandstone-groundwater reaction.

According to previous studies related to geochemical reactions, the weathering process of the reservoir rock after scCO_2 injection was closely related to the surface roughness change of the rock because dissolution and precipitation occur simultaneously and lead to surface roughness change until the geochemical system turns back to a status of equilibrium [22,49]. To observe the surface roughness change of sandstone slabs during the geochemical reaction, seven minerals, quartz, perthite, plagioclase, muscovite, calcite, biotite, and chlorite for each slab surface were determined using a reflecting microscope (Nikon eclipse LV100N, Nikon, Fukasawa, Japan), and three locations for each mineral were randomly selected to acquire 3-dimensional surface images. Each slab was taken out from the cell and dried in an oven at certain reaction time intervals. Then, a total of 262,144 points (512×512) around each selected location (the certain surface domain of $50 \times 50 \mu\text{m}$) of the slab were scanned by an SPM (Scanning Probe Microscope; Icon-PT-PLUS, Bruker, Bremen, Germany). The SPM included a cantilever tip connected to a probe with the laser beam, which was used to measure the height difference at each point and at the standard level (mean height), in nanometers, finally acquiring a 3-dimensional surface image profile for the certain surface domain of a slab (Figure 3). The information acquired from SPM analysis is useful not only for the surface image but also for more quantitative parameters to evaluate the roughness degree of the surface [50,51]. Several surface roughness parameters have been developed, and in this study, a surface roughness value (SR_{RMS}) was used to reduce all of the information in the 3-dimensional surface image to a single number representing the degree of the surface roughness [52,53]. For this study, the SR_{RMS} for the specific surface domain on each slab was calculated from the RMS (root mean square), for which the data can be acquired by measuring the height difference between the standard level (Z_0 is the mean height from all points in a surface domain) and the height of each point in a domain [52].

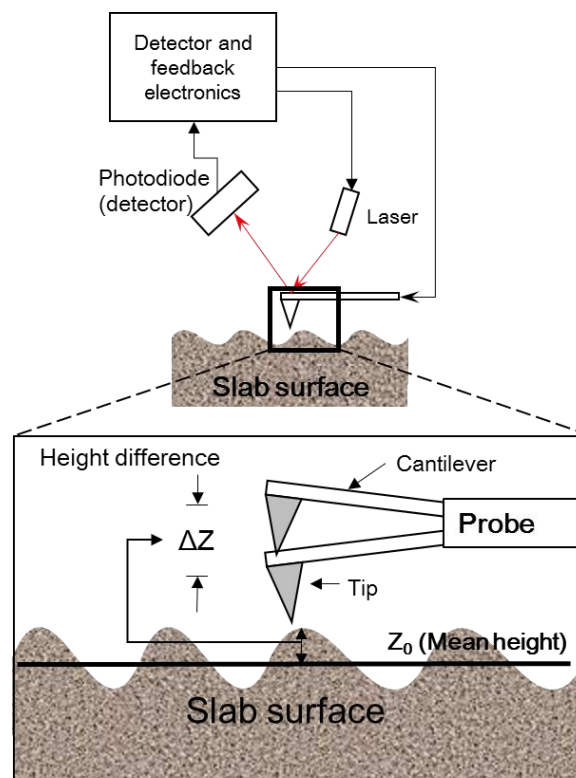


Figure 3. Schematic of the SPM (Scanning Probe Microscope) analysis to calculate SR_{RMS} (surface roughness value).

The following equation was used to calculate the SR_{RMS} (unit: μm) for a specific surface domain:

$$SR_{RMS} = \sqrt{\frac{1}{n} \sum_{i=1}^n \Delta z_i^2} \quad (1)$$

where n is the total point number (262,144) in the surface domain, and Δz_i is the vertical height difference from the mean height (Z_0) to the i th point in the domain [54].

The degree to which the initial surface roughness differed from the reacted surface roughness at a certain reaction time was determined by comparing their SR_{RMS} values. The interrelationship between the degree of the surface roughness and the extent of the geochemical reaction was investigated and the potential application of SR_{RMS} to quantify the weathering process originating from the scCO_2 -sandstone-groundwater reaction was also evaluated by the experiment. The SR_{RMS} values acquired from all minerals' SR_{RMS} values were plotted at different reaction times, and the trend of SR_{RMS} change was compared with the trend of the physical property change of sandstones and the cation concentration change in groundwater, which verified that the surface roughness change reflects the extent of the geochemical weathering process and the rock property change. To verify that the scCO_2 -sandstone-groundwater reaction occurs actively, SEM/EDS analyses for the slab surface were performed and the mineralogical transfer and compositional change on the slab surface were investigated. Three milliliters of groundwater were sampled from the cell at different reaction times (maximum of 150 days) for the chemical analysis, and the same amount of groundwater was added into the cell. The pH and the concentrations of six main cations (Al^{3+} , Ca^{2+} , Fe^{2+} , K^+ , Na^+ , and Si^{4+}) in the groundwater sample were analyzed via ICP/AES (Inductively Coupled Plasma/Atomic Emission Spectrometer; Optima 7300V, Perkin Elmer, Waltham, MA, USA) and using a pH meter, and they were plotted at different reaction times (0–150 reaction days). The relationship among pH change, cation concentration change, physical property change, and SR_{RMS} change was investigated to verify the feasibility of SR_{RMS} usage as a parameter to quantify the extent of the geochemical reaction.

2.3. Measurement of Physical Property Changes for the Sandstone Cores

Several previous studies confirmed that physical properties, such as the porosity, density, and seismic wave velocity of CO_2 reservoir rock can change after CO_2 injection into the reservoir formation [23,32,38,55]. However, it has not been clearly proved what the main reason is for the property change of the reservoir rock and how the change proceeds so rapidly. It is important to quantify the extent of the rock property change because it can affect both leakage safety and CO_2 storage capacity of the reservoir. Changes in porosity, density, and Primary/Secondary (P/S) seismic velocity for nine sandstone cores were measured at different scCO_2 -core-groundwater reaction times, and the results were compared with those of the SR_{RMS} results. To quantify the physical property changes of three sandstones (S1, S2, and S3) due to the geochemical reaction, each core (three cores for each sandstone) was placed in a large stainless steel chamber (1.5 L of capacity), and 1 L of groundwater was added at 100 bar and 50 °C. Then, scCO_2 was injected into the chamber by a high-pressure syringe pump to fill the empty space of the chamber. The inside pressure of the chamber was maintained at 100 bar by a back-pressure controller and the chamber was coated with a heating jacket at 50 °C to maintain the CO_2 as a super critical fluid during the whole reaction time. After each core was taken from the chamber and dried in an oven, the physical properties of the core were measured at different reaction times (total 150 reaction days). The control experiment without scCO_2 in the chamber (zero air instead) was also repeated to separate the effects of scCO_2 injection on rock property changes. Dry density, porosity, and seismic velocity of the cores were measured by the "ASTM/C97" test, "ASTM/C97M-09" test, and "ASTM/D2845-08" test referred from the American Society of Testing Materials. A more detailed procedure for the core experiment can be found in [54]. The property values for the three sandstones vs. reaction time were plotted and their changes were also compared with

those of SR_{RMS} and the cation concentration in groundwater. The schematic of the core experiment to measure the physical property changes of sandstone is shown in Figure 4.

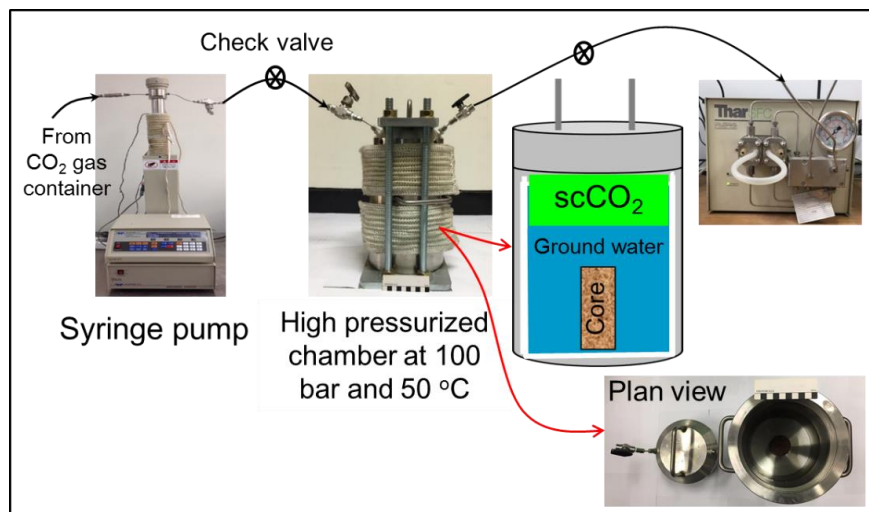


Figure 4. Schematic of the sandstone core experiment for physical property changes.

3. Results and Discussion

3.1. Measurement of the Surface Roughness Value for the Sandstone Slabs

Three-dimensional SPM surface images of the sandstone slab before and after the reaction confirmed that the serious surface roughness change occurred rapidly by the scCO₂-sandstone-groundwater reaction (Figure 5). As seen by comparison with the initial surface, the polished surface of three major minerals (quartz, plagioclase, and biotite) transformed into a bumpy surface at 120 reaction days, suggesting that the weathering processes such as dissolution and precipitation actively occurred on the mineral surfaces of the S1 sandstone, directly increasing the surface roughness. SPM analysis of the calcite surfaces for the sandstone slabs was impossible because the calcites were perforated or seriously damaged by dissolution within 30 reaction days. Results of the SPM image analyses confirmed that the scCO₂-groundwater-sandstone reaction directly resulted in a surface roughness change of the sandstones.

The SR_{RMS} values for three different locations of three minerals for the three sandstone slabs were used to estimate the extent of the surface weathering process of the sandstone at different reaction times. A total of nine SR_{RMS} values for each sandstone slab at a certain reaction time and their average value for each sandstone (S1, S2, and S3) are shown in Table 3 and all the SR_{RMS} values are plotted in Figure 6. In the case of the S1 slab, the average SR_{RMS} of quartz increased from 0.573 to 1.293 μm within 30 reaction days, and the rate of the change became gradually stable after 60 days (Table 3). The average SR_{RMS} of plagioclase and biotite also increased from 0.344 and 0.772 μm to 1.905 and 1.485 μm , respectively, within 30 days, and their SR_{RMS} values gently increased after 60 days. The trends of the SR_{RMS} change for the S2 and the S3 slabs were very similar to that for the S1 slab. The results suggest that the surface roughness increased actively at the early reaction stage, but the change in roughness stabilized after a few months of reaction.

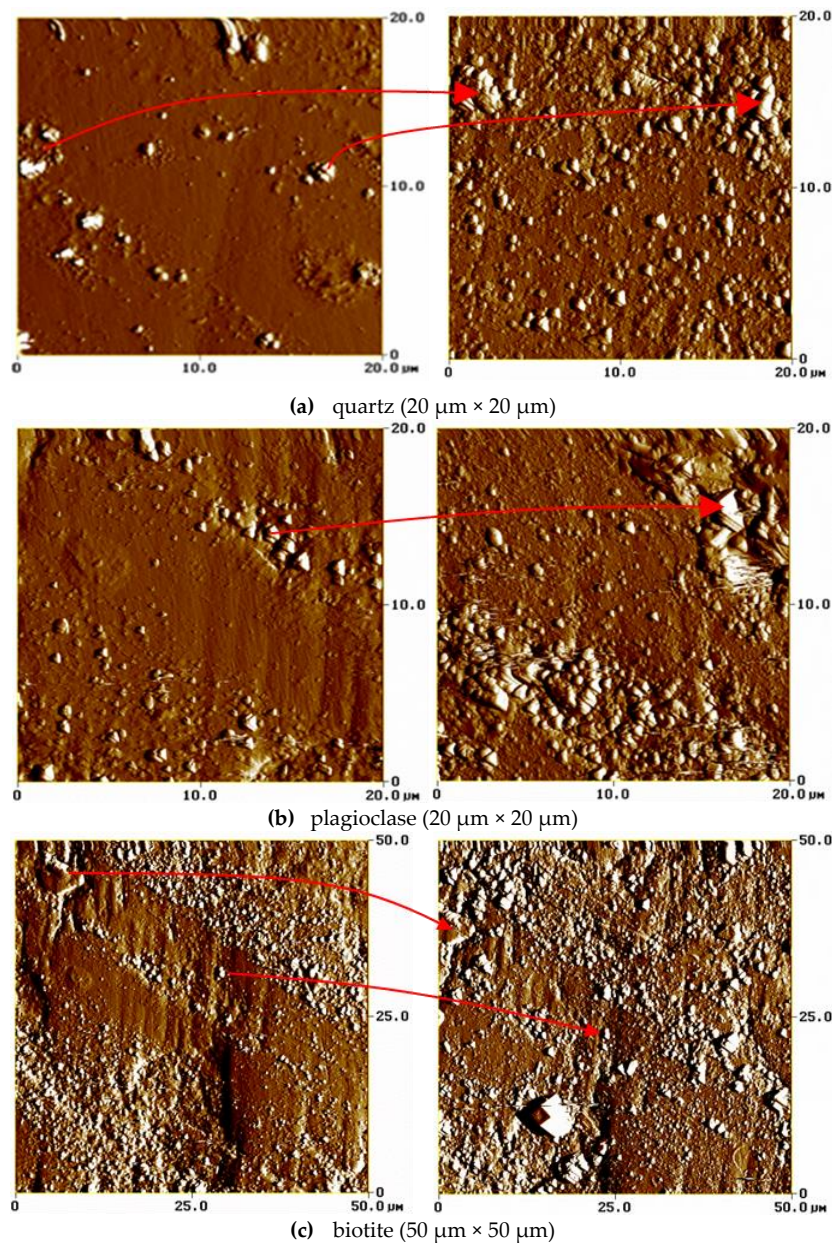


Figure 5. Scanning Probe Microscope (SPM) images of three mineral surfaces for the S1 slab before (left) and after 120 reaction days (right).

Table 3. SR_{RMS} (unit: μm) vs. reaction time for the three sandstone slabs.

Slab Type	Mineral Type	Reaction Time (day)					
		0	10	20	30	60	90
S1	Quartz-1	0.878	1.057	1.176	1.136	1.223	1.261
	Quartz-2	0.322	1.164	1.438	1.541	1.441	1.446
	Quartz-3	0.518	0.945	0.976	1.201	1.242	1.041
	Plagioclase-1	0.164	1.007	1.012	1.711	1.143	2.017
	Plagioclase-2	0.442	1.598	1.133	1.748	2.760	3.068
	Plagioclase-3	0.427	1.130	1.294	1.905	2.160	3.391
	Biotite-1	0.908	1.173	1.752	2.052	1.815	2.091
	Biotite-2	0.749	0.994	1.259	1.078	1.612	2.071
	Biotite-3	0.658	1.250	1.435	1.326	1.273	1.297
S1 average \pm std		0.563 ± 0.25	1.146 ± 0.20	1.275 ± 0.24	1.522 ± 0.35	1.630 ± 0.54	1.965 ± 0.82

Table 3. Cont.

Slab Type	Mineral Type	Reaction Time (day)					
		0	10	20	30	60	90
S1	Quartz-1	0.878	1.057	1.176	1.136	1.223	1.261
	Quartz-2	0.322	1.164	1.438	1.541	1.441	1.446
	Quartz-3	0.518	0.945	0.976	1.201	1.242	1.041
	Plagioclase-1	0.164	1.007	1.012	1.711	1.143	2.017
	Plagioclase-2	0.442	1.598	1.133	1.748	2.760	3.068
	Plagioclase-3	0.427	1.130	1.294	1.905	2.160	3.391
	Biotite-1	0.908	1.173	1.752	2.052	1.815	2.091
	Biotite-2	0.749	0.994	1.259	1.078	1.612	2.071
	Biotite-3	0.658	1.250	1.435	1.326	1.273	1.297
S1 average ± std		0.563 ± 0.25	1.146 ± 0.20	1.275 ± 0.24	1.522 ± 0.35	1.630 ± 0.54	1.965 ± 0.82
S2	Quartz-1	0.275	0.169	1.612	1.512	1.997	2.011
	Quartz-2	0.276	0.663	1.035	1.362	1.540	1.581
	Quartz-3	0.271	0.590	1.274	1.420	2.055	1.998
	Plagioclase-1	0.157	0.436	1.287	1.909	1.201	2.318
	Plagioclase-2	0.192	1.151	1.205	1.955	1.854	2.101
	Plagioclase-3	0.184	0.840	1.203	1.679	1.788	1.991
	Biotite-1	0.698	1.166	1.988	1.747	1.689	2.485
	Biotite-2	0.666	1.122	1.131	1.244	1.215	1.303
	Biotite-3	0.612	0.746	1.499	1.585	1.810	2.13
S2 average ± std		0.370 ± 0.22	0.765 ± 0.34	1.359 ± 0.30	1.601 ± 0.24	1.683 ± 0.31	1.991 ± 0.36
S3	Quartz-1	0.259	0.681	0.702	0.739	0.865	0.998
	Quartz-2	0.142	0.661	0.898	0.980	0.939	1.103
	Quartz-3	0.226	0.571	0.860	0.801	0.888	0.998
	Plagioclase-1	0.084	0.623	0.635	0.684	0.754	1.774
	Plagioclase-2	0.224	0.922	0.600	0.635	1.189	1.696
	Plagioclase-3	0.196	0.702	0.852	0.843	0.828	1.033
	Biotite-1	0.554	0.782	1.110	1.017	1.358	1.551
	Biotite-2	0.394	0.656	0.797	0.836	1.179	0.966
	Biotite-3	0.362	0.804	0.977	0.955	0.899	0.954
S3 average ± std		0.271 ± 0.14	0.711 ± 0.11	0.826 ± 0.16	0.832 ± 0.13	0.989 ± 0.20	1.230 ± 0.25

Figure 6 shows the average SR_{RMS} for the three sandstones at different reaction days, comparing SR_{RMS} with the control slab (S1 slab reacted with only groundwater). The increase in the average SR_{RMS} for the S1 slab with only groundwater was negligible for 120 reaction days (only a 2.8% increase). However, the average SR_{RMS} for the S1 slab with $scCO_2$ and groundwater increased by 2.5 times during 120 reaction days and 4.4 and 3.5 times for the S2 and the S3 slab, respectively. For all three sandstones with the $scCO_2$ and groundwater reaction, the average SR_{RMS} increased precipitously for 30 days of the reaction. After 60 days of the reaction, the SR_{RMS} increase became less severe, suggesting that no more serious increase in surface roughness occurred. For quantitative analysis of the surface roughness change for the three sandstones (S1, S2, and S3), the curve fitting results for their SR_{RMS} values using the logarithmic Equation (2) are delineated in Figure 6:

$$SR_{RMS}(t) = a \ln(t) + b \tag{2}$$

where t is the reaction time (day); a is the rate constant of the surface roughness change; and b is the intercept constant [54]. The r -square values for all fitted curves are higher than 0.83 (average of 0.891 in Figure 6), indicating that the SR_{RMS} change follows a well-defined logarithmic pattern.

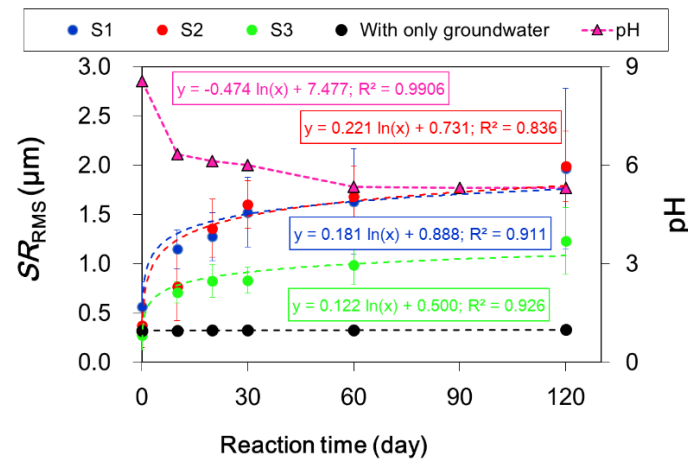


Figure 6. The SR_{RMS} and pH change by the $scCO_2$ -sandstone-groundwater reaction.

The pH of the groundwater decreased to 5.3 due to the dissolved $scCO_2$, which led to the dissolution of the sandstone slab in groundwater, but it became stable after 60 reaction days, suggesting that the amount of hydrogen ions in the groundwater increased due to the dissolution of CO_2 at an early stage, but the pH levels remained stable due to the buffering of dissolved ions with the increase of the reaction time (within 90–120 days). The trend of the pH decrease in the groundwater vs. the reaction time was also very similar to that of the SR_{RMS} increase of the slabs (the logarithmic decrease (or increase) pattern in Figure 6), indicating that the geochemical weathering process of the sandstone reservoir was very active in the early CO_2 injection time but stabilized within a few months. If the trend of the $scCO_2$ involved geochemical reaction is similar to that of the SR_{RMS} , the surface roughness change could be used to quantify the extent of the $scCO_2$ -rock-groundwater reaction.

In this study, the trend of the dissolved ion concentration change in the groundwater during the $scCO_2$ -involved reaction was also compared to the trend of the SR_{RMS} and pH change. The concentration of five cations in the groundwater during the reaction is shown in Figure 7.

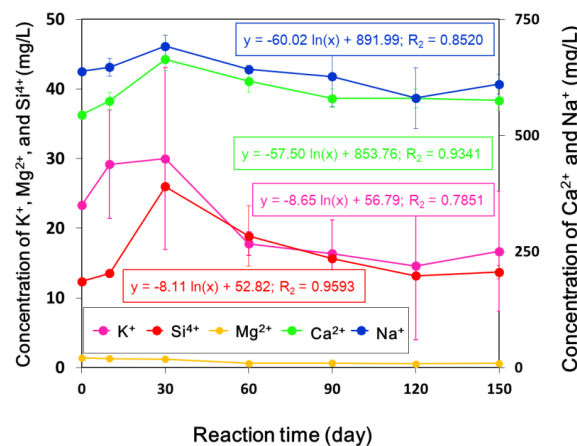


Figure 7. Concentration change of five cations in the groundwater during the $scCO_2$ involved reaction (trend lines calculated from the data after 30 days).

The average K^+ and Si^{4+} concentrations in the groundwater increased from 23.3 and 12.4 mg/L to 30.0 and 26.0 mg/L after 30 reaction days, respectively, and were then stabilized by gradually decreasing after 90 days. The results suggest that the concentration of K^+ and Si^{4+} mainly increased by the dissolution of silicate minerals such as K-feldspar and then decreased by the precipitation of secondary minerals, including K^+ ions (this is also supported by SEM/EDS analyses in Figures 8

and 9). The average concentration of Ca^{2+} and Na^+ increased from 547.1 and 633.2 mg/L to 663.8 and 692.0 mg/L after 30 days, respectively. However, after 90 days, they gradually decreased to 579.4 and 627.0 mg/L. The results showed that most minerals in the sandstone slab had a tendency to dissolve in the groundwater during the early reaction days (about 30–60 days), but the dissolution became stable after 90 days of reaction, resulting from the secondary precipitations overcoming the continuous dissolution during the geochemical reaction in the cell. The trend of cation concentration change in the groundwater after 30 days was also similar to those of the SR_{RMS} and pH change during the scCO_2 -sandstone-groundwater reaction, showing an interesting possibility for the use of SR_{RMS} change of the rock surface to estimate the process of the geochemical reaction (Figure 7). From these comparisons of trends, it was concluded that the dissolution process of the CO_2 reservoir sandstones was dominant at the early CO_2 injection time (less than 60 days), but precipitation also occurred sequentially to decrease the concentrations of dissolved ions and to stabilize the unbalanced geochemical system within a few months after CO_2 injection.

To identify the weathering process of the reservoir rock by the scCO_2 -reservoir rock-groundwater reaction, the surfaces of the S1-1 sandstone slab were analyzed using SEM/EDS before the reaction and after 120 reaction days and their SEM images are shown in Figure 8.

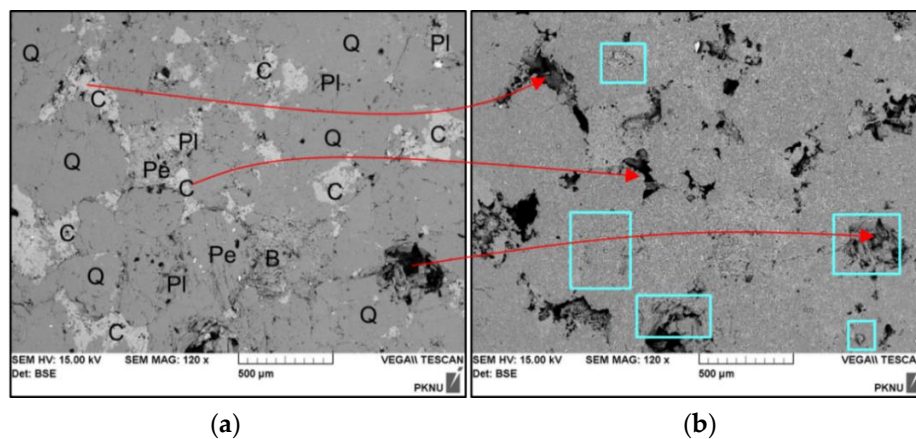


Figure 8. Scanning Electron Microscope (SEM) images of the S1-1 slab surface (a) before and (b) after 120 reaction days (Q: quartz, Pl: plagioclase, Pe: perthite, B: biotite, C: calcite, and □: secondary precipitates).

The SEM images show that the slab surface was heavily deformed by the geochemical reaction and the weathering process actively occurred along the existing fractures or mineral boundaries. The crack that existed at the mineral boundaries before the reaction was clearly expanded, and the calcites were perforated by the dissolution during the reaction, suggesting that these geochemical weathering processes can increase the porosity or the permeability of the reservoir rocks (this is discussed in detail in Section 3.2). In contrast, some pre-existing pores on the mineral surface were filled with secondary precipitates after the reaction, and additional precipitation on mineral surfaces such as quartz and biotite also occurred (Figure 8). The typical precipitates created on the S2-1 and S3-1 slab surfaces were analyzed using SEM/EDS after 120 reaction days, where they were determined to be amorphous silicate minerals as well as calcite, halite, and kaolinite, mostly consisting of Si^{4+} , Na^+ , K^+ , Ca^{2+} , Al^{3+} , and Fe^{2+} (Figure 9). These SEM/EDS analyses also indicated that both dissolution and precipitation occur on the sandstone surface due to the weathering process during the scCO_2 -rock-groundwater reaction, which directly caused the roughness change of the rock surface and which represented the extent of the geochemical reaction over the reaction time. If these experimental results confirm that the SR_{RMS} change is directly proportional to the extent of the geochemical reaction, the trend of the SR_{RMS} change can be used to estimate the progress of the reaction, which mostly results from dissolution and precipitation. If the active dissolution and precipitation of sandstones occur over a short period of

reaction time, accompanying the SR_{RMS} and physical property changes when CO_2 is injected into the sandstone reservoir, the activity of the geochemical reaction is likely to be an important parameter in determining the optimal CO_2 injection site, and further studies will be necessary to conclusively link the extent and influence with leakage safety of CO_2 sequestration.

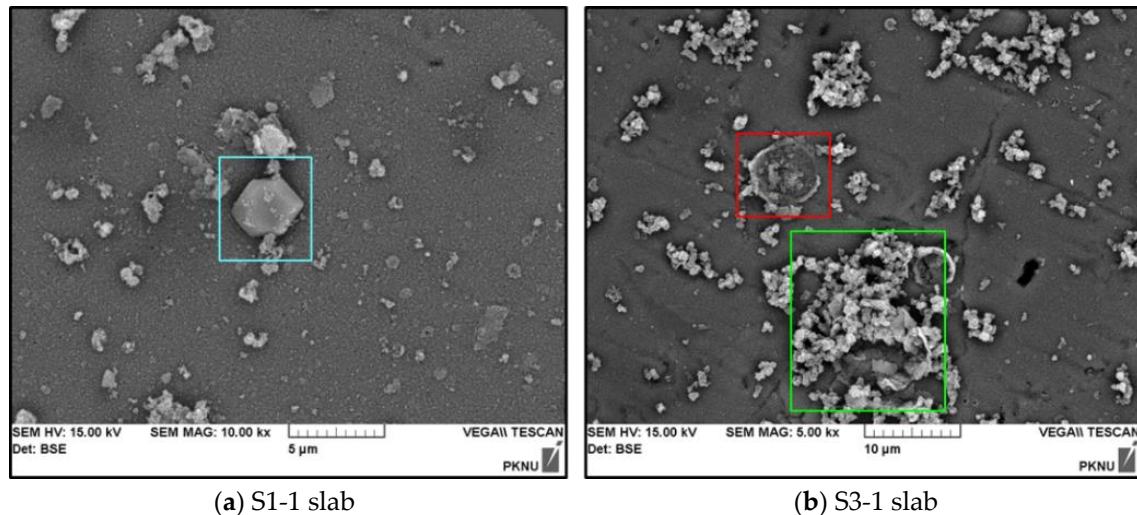


Figure 9. SEM images for precipitates created on the slab surface after 120 reaction days (□: halite, □: calcite, and □: amorphous silicate minerals).

3.2. Measurement of Physical Property Changes for the Sandstone Cores

Table 4 shows the porosity changes for the three sandstones (total nine cores) vs. the reaction time (total of 150 days). The initial average porosity of the S1 sandstone cores was 8.097%, and it increased to 8.642% after 150 reaction days (6.7% increase from the initial value). The average porosity of the S2 and S3 sandstones also increased to 8.2% and 9.9% compared with the initial values, respectively. Even though the porosity increase of the rock cores occurred at the early stage of the reaction because of crack extension and perforation dominated by the dissolution, this was moderated within a few months, showing a logarithmic increase vs. reaction time (Figure 10a). The average dry density of the sandstone cores decreased from 2.390 to 2.384 g/cm^3 for 120 reaction days (0.25% decrease from the initial value) (Table 5). The average seismic wave velocities of the sandstones also decreased in a logarithmic manner to 5.67% for P-wave and to 5.75% for S-wave from the initial values for 150 reaction days (Figure 10b and Table 5). The decrease in the dry density and seismic wave velocity for the sandstones was associated with an increase in porosity due to the geochemical weathering process during the reaction, which considers their interrelation characteristics. For a more quantitative analysis of the physical property changes for the nine sandstone cores, the curve fitting results for their property values using the logarithmic Equation (2) are delineated in Figure 10. The r -squared values for all fitted curves are higher than 0.88 (average of 0.921), indicating that the rock property changes follow a well-defined logarithmic increase (or decrease) pattern, which were very similar to those of the geochemical parameter changes such as pH, cation concentration, and SR_{RMS} over the reaction time.

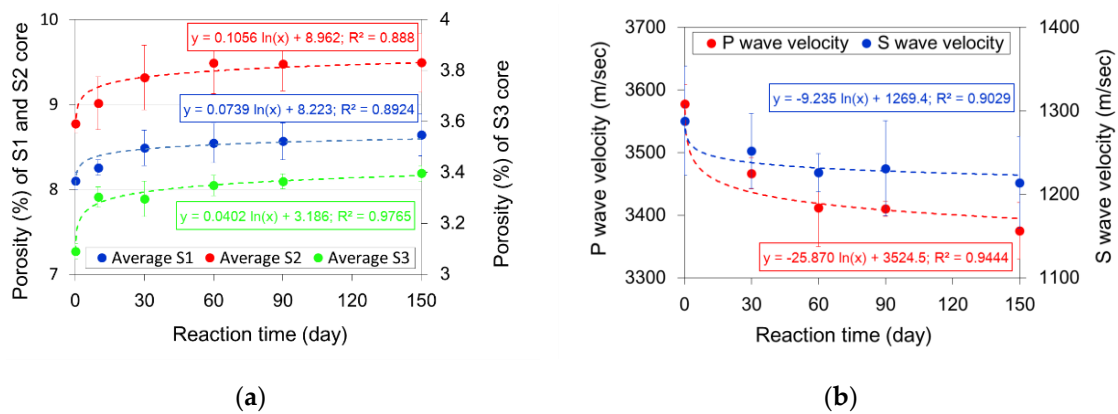


Figure 10. Average porosity change (a) and average seismic wave velocity change (b) for the sandstone cores during the scCO₂-sandstone-groundwater reaction.

Table 4. Porosity change for the three sandstone cores for 150 reaction days.

Sandstone	Reaction Time (day)						Porosity Change Rate (%) during 150 Days ⁽¹⁾
	0	10	30	60	90	150	
S1	8.183	8.321	8.464	8.569	8.553	8.649	5.7
	8.121	8.149	8.293	8.299	8.350	8.39	3.3
	7.986	8.298	8.705	8.767	8.791	8.888	11.3
S1 average ± std	8.097 ± 0.10	8.256 ± 0.09	8.487 ± 0.21	8.545 ± 0.23	8.565 ± 0.22	8.642 ± 0.25	6.7
S2	8.760	8.991	9.360	9.460	9.462	9.459	8.0
	8.889	9.334	9.673	9.857	9.811	9.859	10.9
	8.680	8.713	8.919	9.148	9.163	9.160	5.5
S2 average ± std	8.776 ± 0.11	9.013 ± 0.31	9.318 ± 0.38	9.488 ± 0.36	9.479 ± 0.32	9.493 ± 0.35	8.2
S3	3.121	3.278	3.221	3.305	3.353	3.412	9.3
	3.056	3.282	3.33	3.38	3.336	3.358	9.9
	3.093	3.349	3.337	3.361	3.402	3.419	10.5
S3 average ± std	3.090 ± 0.03	3.303 ± 0.04	3.296 ± 0.07	3.349 ± 0.04	3.364 ± 0.03	3.396 ± 0.03	9.9

$$* (1): \left| \frac{\text{value for 150 day} - \text{value for 0 day}}{\text{value for 0 day}} \right| \times 100.$$

Table 5. Average density and seismic wave velocity changes for the three sandstones during the reaction.

Property	Reaction Time (day)					Property Change Rate (%) during 150 Days ⁽¹⁾
	0	30	60	90	150	
Dry density (g/cm ³)	2.390 ± 0.0003	2.387 ± 0.0007	2.386 ± 0.0003	2.384 ± 0.0004	2.384 ± 0.0008	0.25
P-wave velocity (m/s)	3.578 ± 31	3.467 ± 25	3.412 ± 62	3.410 ± 12	3.375 ± 45	5.67
S-wave velocity (m/s)	1.288 ± 65	1.252 ± 45	1.226 ± 23	1.231 ± 57	1.214 ± 55	5.75

$$* (1): \left| \frac{\text{value for 150 day} - \text{value for 0 day}}{\text{value for 0 day}} \right| \times 100.$$

These similarities are evidence demonstrating that the rock property change directly originated from the geochemical reaction with the injected scCO₂, which further resulted in the rock surface roughness change and ion concentration change in the groundwater, and also that the surface roughness measurement provides a lot of quantitative information regarding the extent of the geochemical reaction related to the scCO₂ in the subsurface. The results showed that the physical properties of the sandstone changed rapidly within a few months due to the geochemical reaction with the injected CO₂, but the rate decreased in a relatively short time (a few months), verifying that the physical property change of the CO₂ reservoir rocks occurred faster than expected from previous research [56–58]. Because the effect of the geochemical reaction on the reservoir rock property change is moderated after a short time, attention to the geochemical reaction at the early CO₂ injection stage is very important in preventing leakage and in understanding CO₂ sequestration site characteristics from the CO₂ storage capacity point of view.

4. Conclusions

During the last decade, one of the main issues for CO₂ storage sites has been how the scCO₂ involved geochemical reaction affects the storage capacity and the leakage safety after scCO₂ injection into the subsurface. Several studies confirmed that the geochemical reaction rate was much faster than expected. Such findings suggested the possibility that the geochemical reaction may generate further changes in the reservoir rock properties. For a specific CO₂ storage site, it becomes very important to evaluate whether or not the geochemical reaction is significant enough to threaten the leakage safety of the CO₂ sequestration site. Through a novel approach for determining the correlations among changes in SR_{RMS} , physical properties, pH, and dissolved cation concentration in the groundwater during the scCO₂-rock-groundwater reaction, this study successfully verified the potential of using SR_{RMS} values as a new parameter to quantify the extent of a geochemical reaction.

For sandstone sites in the Gyeongsang basin of South Korea, the trends of several property changes originating from the scCO₂ involved reaction displayed similar logarithmic patterns, which confirmed that the scCO₂-sandstone-groundwater reaction occurs actively in the early CO₂ injection stage (a few months), but it then becomes stable and further rock property changes are halted. As a result of this study, the CO₂ sequestration site in the Gyeongsang basin can be evaluated as an appropriate site from the viewpoint of geochemical safety if a careful observation over the geochemical reaction in the early CO₂ injection stage is performed. The use of SR_{RMS} values to evaluate the extent of the geochemical reaction will be available for any other CO₂ site in the world to secure leakage safety for reservoirs or formations.

Acknowledgments: This research was supported by a grant (16CTAP-C115166-01) from the Technology Advancement Research Program (TARP) funded by the Ministry of Land, Infrastructure, and Transport of the Korean government. The authors would like to express their gratitude to the anonymous reviewers for their critical comments and advice.

Author Contributions: Minhee Lee and Jinyoung Park conceived and designed the experiments; Jinyoung Park and Kyoungbae Baek performed the experiments and the data analyses; Sookyun Wang and Chul-Woo Chung contributed materials and data interpretation; Minhee Lee wrote the paper.

Conflicts of Interest: The authors declare no conflict of interest.

References

1. Safdarmejad, M.; Hedengren, D.; Baxter, L. Dynamic optimization of a hybrid system of energy-storing cryogenic carbon capture and a baseline power generation unit. *Appl. Energy* **2016**, *172*, 66–79. [[CrossRef](#)]
2. Gopan, A.; Kumfer, M.; Phillips, J.; Thimsen, D.; Smith, R.; Axelbaum, R.L. Process design and performance analysis of a Staged, Pressurized Oxy-Combustion (SPOC) power plant for carbon capture. *Appl. Energy* **2014**, *125*, 179–188. [[CrossRef](#)]
3. Cohen, M.; Rochelle, T.; Webber, E. Optimizing postcombustion CO₂ capture in response to volatile electricity prices. *Int. J. Greenh. Gas Control* **2012**, *8*, 180–195. [[CrossRef](#)]
4. Bachu, S.; Gunter, D.; Perkins, H. Aquifer disposal of CO₂: Hydrodynamic and mineral trapping. *Energy Convers. Manag.* **1994**, *35*, 269–279. [[CrossRef](#)]
5. Gunter, D.; Perkins, H.; McCann, J. Aquifer disposal of CO₂-rich gases, reaction design for added capacity. *Energy Convers. Manag.* **1993**, *3*, 941–948. [[CrossRef](#)]
6. International Energy Agency (IEA). *World Energy Outlook 2010*; Annual Report; OECD/IEA: Paris, France, 2010.
7. Holloway, S. An overview of the underground disposal of CO₂. *Energy Convers. Manag.* **1997**, *3*, 193–198. [[CrossRef](#)]
8. Klara, M.; Srivastava, D.; McIlvried, G. Integrated collaborative technology development program for CO₂ sequestration in geologic formations-United States Department of Energy R&D. *Energy Convers. Manag.* **2003**, *44*, 2699–2712. [[CrossRef](#)]
9. Ampomah, W.; Balch, R.; Cather, M.; Rose-Coss, D.; Dai, Z.; Heath, J.; Dewers, T.; Mozley, P. Evaluation of CO₂ storage mechanisms in CO₂ enhanced oil recovery sites: Application to Morrow sandstone reservoir. *Energy Fuels* **2016**, *30*, 8545–8555. [[CrossRef](#)]

10. Dai, Z.; Viswanathan, H.; Middleton, R.; Pan, F.; Ampomah, W.; Yang, C.; Jia, W.; Xiao, T.; Lee, S.; McPherson, B.; et al. CO₂ accounting and risk analysis for CO₂ sequestration at enhanced oil recovery sites. *Environ. Sci. Technol.* **2016**, *50*, 7546–7554. [[CrossRef](#)] [[PubMed](#)]
11. Pan, F.; McPherson, J.; Dai, J.; Jia, W.; Lee, S.; Ampomah, W.; Viswanathan, H.; Esser, R. Uncertainty analysis of carbon sequestration in an active CO₂-EOR field. *Int. J. Greenh. Gas Control* **2016**, *51*, 18–28. [[CrossRef](#)]
12. Kirste, D.; Haese, R.; Boreham, C.; Schacht, U. Evolution of formation water chemistry and geochemical modeling of the CO₂CRC Otway site residual gas saturation test. *Energy Proc.* **2014**, *63*, 2894–2902. [[CrossRef](#)]
13. Mito, S.; Xue, Z.; Ohsumi, T. Case study of geochemical reactions at the Nagaoka CO₂ injection site, Japan. *Int. J. Greenh. Gas Control* **2008**, *2*, 309–318. [[CrossRef](#)]
14. Neele, F.; Quinquis, H.; Read, A.; Wright, M.; Lorsche, J.; Poulussen, D.F. CO₂ storage development: Status of the large European CCS projects with EPR funding. *Energy Proc.* **2014**, *63*, 6053–6066. [[CrossRef](#)]
15. Zhang, K.; Xie, J.; Li, C.; Hu, L.; Wu, X.; Wang, Y. A full chain CCS demonstration project in northeast Ordos basin, China: Operational experience and challenges. *Int. J. Greenh. Gas Control* **2016**, *50*, 218–230. [[CrossRef](#)]
16. Miocic, J.M.; Gilfillan, S.M.V.; Roberts, J.J.; Edlmann, K.; McDermott, C.I.; Haszeldine, R.S. Controls on CO₂ storage security in natural reservoirs and implications for CO₂ storage site selection. *Int. J. Greenh. Gas Control* **2016**, *51*, 118–125. [[CrossRef](#)]
17. Pereira, N.; Carneiro, J.F.; Araújo, A.; Bezzeghoud, M.; Borges, J. Seismic and structural geology constraint to the selection of CO₂ storage sites-The case of the onshore Lusitanian basin, Portugal. *J. Appl. Geophys.* **2014**, *102*, 21–38. [[CrossRef](#)]
18. Gunter, W.D.; Wiwehar, B.; Perkins, E.H. Aquifer disposal of CO₂-rich greenhouse gases: Extension of the time scale of experiment for CO₂-sequestering reactions by geochemical modeling. *Mineral. Petrol.* **1997**, *59*, 121–140. [[CrossRef](#)]
19. Koide, G.; Takahashi, M.; Tsukamoto, H. Self-trapping mechanisms of carbon dioxide. *Energy Convers. Manag.* **1995**, *36*, 505–508. [[CrossRef](#)]
20. Perkins, E.; Lauriol, C.; Azaroual, M.; Durst, P. Long term predictions of CO₂ storage by mineral and solubility trapping in the Weyburn Midale Reservoir. In Proceedings of the 7th International Conference on Greenhouse Gas Control Technologies (GHGT-7), Vancouver, BC, Canada, 5–9 September 2004; pp. 2093–2096.
21. Kampman, N.; Bickle, M.; Wigley, M.; Dubacq, B. Fluid flow and CO₂-fluid-mineral interactions during CO₂-storage in sedimentary basins. *Chem. Geol.* **2014**, *369*, 22–50. [[CrossRef](#)]
22. Kang, H.; Baek, K.; Wang, S.; Park, J.; Lee, M. Study on the dissolution of sandstones in Gyeongsang basin and the calculation of their dissolution coefficients under CO₂ injection condition. *Econ. Environ. Geol.* **2012**, *45*, 661–672. [[CrossRef](#)]
23. Park, J.; Baek, K.; Lee, M.; Wang, S. Physical property changes of sandstones in Korea derived from the supercritical CO₂-sandstone-groundwater geochemical reaction under CO₂ sequestration condition. *Geosci. J.* **2015**, *19*, 313–324. [[CrossRef](#)]
24. Pham, P.; Lu, P.; Agraard, P.; Zhu, C.; Hellevang, H. On the potential of CO₂-water-rock interactions for CO₂ storage using a modified kinetic model. *Int. J. Greenh. Gas Control* **2011**, *5*, 1002–1015. [[CrossRef](#)]
25. Wang, T.; Wang, H.; Zhang, F.; Xu, T. Simulation of CO₂-water-rock interactions on geologic CO₂ sequestration under geological conditions of China. *Mar. Pollut. Bull.* **2013**, *76*, 307–314. [[CrossRef](#)] [[PubMed](#)]
26. Yu, Z.; Liu, L.; Yang, S.; Li, S.; Yang, Y. An experimental study of CO₂-brine-rock interaction at in situ pressure-temperature reservoir conditions. *Chem. Geol.* **2012**, *326*, 88–101. [[CrossRef](#)]
27. Cao, P.; Karpyn, T.; Li, L. The role of host rock properties in determining potential CO₂ migration pathways. *Int. J. Greenh. Gas Control* **2016**, *45*, 18–26. [[CrossRef](#)]
28. Yasuhara, H.; Kinoshita, N.; Lee, D.S.; Choi, J.; Kishida, K. Evolution of mechanical and hydraulic properties in sandstone induced by simulated mineral trapping of CO₂ geo-sequestration. *Int. J. Greenh. Gas Control* **2017**, *56*, 155–164. [[CrossRef](#)]
29. Zhang, K.; Cheng, Y.; Li, W.; Wu, D.; Liu, Z. Influence of supercritical CO₂ on pore structure and functional groups of coal: Implications for CO₂ sequestration. *J. Nat. Gas Sci. Eng.* **2017**, *40*, 288–298. [[CrossRef](#)]
30. Alonso, J.; Navarro, V.; Calvo, B.; Asensio, L. Hydro-mechanical analysis of CO₂ storage in porous rocks using a critical state model. *Int. J. Rock Mech. Min.* **2012**, *54*, 19–26. [[CrossRef](#)]
31. Auquē, F.; Acero, P.; Gimeno, J.; Gómez, B.; Asta, P. Hydrogeochemical modeling of a thermal system and lessons learned for CO₂ geologic storage. *Chem. Geol.* **2009**, *268*, 324–336. [[CrossRef](#)]

32. Buscheck, A.; Sun, Y.; Chen, M.; Hao, Y.; Wolery, J.; Bourcier, L.; Court, B.; Celia, A.; Friedmann, S.J.; Aines, R.D. Active CO₂, reservoir management for carbon storage: Analysis of operational strategies to relieve pressure buildup and improve injectivity. *Int. J. Greenh. Gas Control* **2012**, *6*, 230–245. [[CrossRef](#)]
33. Choi, Y.; Yun, T.; Mayer, B.; Hong, Y.; Kim, H.; Jo, Y. Hydrogeochemical processes in clastic sedimentary rocks, South Korea: A natural analogue study of the role of dedolomitization in geologic carbon storage. *Chem. Geol.* **2012**, *306*, 103–113. [[CrossRef](#)]
34. Irina, G. Role and impact of CO₂–rock interactions during CO₂ storage in sedimentary rocks. *Int. J. Greenh. Gas Control* **2010**, *4*, 73–89. [[CrossRef](#)]
35. Koornneef, J.; Ramires, A.; Urkenburg, W.; Faaij, A. The environmental impact and risk assessment of CO₂ capture, transport and storage—An evaluation of the knowledge base. *Prog. Energy Combust. Sci.* **2012**, *38*, 62–86. [[CrossRef](#)]
36. Xu, T.; Apps, A.; Pruess, K. Numerical simulation to study mineral trapping for CO₂ disposal in deep aquifers. *Appl. Geochem.* **2004**, *19*, 917–936. [[CrossRef](#)]
37. Bachu, S.; Bonijoly, D.; Bradshaw, J.; Burruss, R.; Holloway, S.; Christensen, P.; Mathiassen, M. CO₂ storage capacity estimation: Methodology and gaps. *Int. J. Greenh. Gas Control* **2007**, *1*, 430–443. [[CrossRef](#)]
38. Berrezueta, E.; González-Menéndez, L.; Breitner, D.; Luquot, L. Pore system changes during experimental CO₂ injection into detritic rocks: Studies of potential storage rocks from some sedimentary basins of Spain. *Int. J. Greenh. Gas Control* **2013**, *17*, 411–422. [[CrossRef](#)]
39. Zhao, F.; Liao, W.; Yin, D. An experimental study for the effect of CO₂-brine-rock interaction on reservoir physical properties. *J. Energy Inst.* **2015**, *88*, 27–35. [[CrossRef](#)]
40. Bader, G.; Thibeau, S.; Vincke, O.; Jannaud, D.; Saysset, S.; Joffre, H.; Giger, M.; David, M.; Gimenez, M.; Dieulin, A.; Copin, D. CO₂ storage capacity evaluation in deep saline aquifers for an industrial pilot selection, methodology and results of the France Nord project. *Energy Proc.* **2014**, *63*, 2779–2788. [[CrossRef](#)]
41. Li, P.; Zhou, D.; Zhang, C.; Chen, G. Assessment of the effective CO₂ storage capacity in the Beibuwan Basin, offshore of southwestern P. R. China. *Int. J. Greenh. Gas Control* **2015**, *37*, 325–339. [[CrossRef](#)]
42. IWR (International Economic Platform for Renewable Energies). Climate: Global CO₂ Emissions Rise to New Record Level in 2011. Pressed on Renewable Energy Industry, Germany. Available online: <http://www.cerina.org/en/co2-global/co2-2011> (accessed on 1 June 2017).
43. Park, Y.; Huh, D.; Yoo, D.; Hwang, S.; Lee, H.; Roh, E. A review of business model for CO₂ geological storage project in Korea. *J. Geol. Soc. Korea* **2009**, *45*, 579–587.
44. Egawa, K.; Hong, S.; Lee, H.; Choi, T.; Lee, M.; Kang, J.; Yoo, K.; Kim, J.; Lee, Y.; Kihm, J.; Kim, J. Preliminary evaluation of geological storage capacity of CO₂ in sandstones of the Sindong Group, Gyeongsang Basin (Cretaceous). *J. Geol. Soc. Korea* **2009**, *45*, 463–472.
45. Alemu, B.L.; Aagaard, P.; Munz, I.A.; Skurtveit, E. Caprock interaction with CO₂: A laboratory study of reactivity of shale with supercritical CO₂ and brine. *Appl. Geochem.* **2011**, *26*, 1975–1989. [[CrossRef](#)]
46. Dawson, W.; Pearce, K.; Biddle, D.; Golding, D. Experimental mineral dissolution in Berea Sandstone reacted with CO₂ or SO₂-CO₂ in NaCl brine under CO₂ sequestration conditions. *Chem. Geol.* **2015**, *399*, 87–97. [[CrossRef](#)]
47. Farquhar, M.; Pearce, K.; Dawson, W.; Golab, A.; Sommacal, S.; Kirste, D.; Biddle, D.; Golding, D. A fresh approach to investigating CO₂ storage: Experimental CO₂-water-rock interactions in a low-salinity reservoir system. *Chem. Geol.* **2015**, *399*, 98–122. [[CrossRef](#)]
48. Liu, F.; Lu, P.; Griffith, C.; Hedges, S.W.; Soong, Y.; Hellevang, H.; Zhu, C. CO₂-brine-caprock interaction: Reactivity experiments on Eau Claire shale and a review of relevant literature. *Int. J. Greenh. Gas Control* **2012**, *7*, 153–167. [[CrossRef](#)]
49. Ko, M.; Kang, H.; Wang, S.; Lee, M. The weathering process of olivine and chlorite reacted with the supercritical CO₂ on the sequestration condition. *J. Geol. Soc. Korea* **2011**, *45*, 463–472.
50. Senetakis, K.; Coop, R.; Todisco, C. The inter-particle coefficient of friction at the contacts of Leighton Buzzard sand quartz minerals. *Soils Found.* **2013**, *53*, 746–755. [[CrossRef](#)]
51. Yang, H.; Baudet, A.; Yao, T. Characterization of the surface roughness of sand particles using an advanced fractal approach. *Proc. R. Soc. A* **2016**, *472*, 1–20. [[CrossRef](#)]
52. Degarmo, P.; Black, T.; Kohser, A. *Materials and Processes in Manufacturing*, 9th ed.; Wiley: New Jersey, NJ, USA, 2003.

53. Den Outer, A.; Kaashoek, F.; Hack, K. Difficulties of using continuous fractal theory for discontinuity surfaces. *Int. J. Rock Mech. Min.* **1995**, *32*, 3–9. [[CrossRef](#)]
54. Lee, M.; Wang, S.; Kim, S.; Park, J. Investigation of the relationship between CO₂ reservoir rock property change and the surface roughness change originating from the supercritical CO₂-sandstone-groundwater geochemical reaction at CO₂ sequestration condition. *Energy Proc.* **2015**, *76*, 495–502. [[CrossRef](#)]
55. Javadpour, F. CO₂ injection in geological formations: Determining macroscale coefficients from pore scale processes. *Transp. Porous Med.* **2009**, *79*, 87–105. [[CrossRef](#)]
56. Kjølner, C.; Weibel, R.; Bateman, K.; Laier, T.; Nielsen, H.; Frykman, P.; Springer, N. Geochemical impacts of CO₂ storage in saline aquifers with various mineralogy—results from laboratory experiments and reactive geochemical modeling. *Energy Proc.* **2011**, *4*, 4724–4731. [[CrossRef](#)]
57. Silva, D.; Ranjith, G.; Perera, A. Geochemical aspects of CO₂ sequestration in deep saline aquifers: A review. *Fuel* **2015**, *155*, 128–143. [[CrossRef](#)]
58. Mitiku, B.; Li, D.; Bauer, S.; Beyer, C. Geochemical modeling of CO₂-water-rock interactions in a potential storage formation of the North German sedimentary basin. *Appl. Geochem.* **2013**, *36*, 168–186. [[CrossRef](#)]



© 2017 by the authors. Licensee MDPI, Basel, Switzerland. This article is an open access article distributed under the terms and conditions of the Creative Commons Attribution (CC BY) license (<http://creativecommons.org/licenses/by/4.0/>).